Trace element variability in titanite from diverse geologic environments

Frank K. Mazdab[1], Joseph L. Wooden[1] & Andrew P. Barth[2]

[1]U.S.G.S.-Stanford Ion Probe Laboratory, Stanford, CA 94305 USA
[2]I.U.P.U.I. Department of Geology, Indianapolis, IN 94305 USA
e-mail: fmazdab@usgs.gov; jwooden@usgs.gov; ibsz100@iupui.edu

The SHRIMP-RG at the U.S.G.S.-Stanford Ion Probe Laboratory in Stanford, California.
http://shrimprg.stanford.edu

Introduction

- Titanite is widespread amongst igneous, metamorphic and metasomatic rocks.
- Titanite incorporates a variety of geologically significant minor and trace elements during growth that may be diagnostic of the local chemical and P-T conditions of its formation.
- *In-situ* micro-analytical measurements permit detailed studies of individual zones within composite grains and minimizes accidental overlap with inclusions.
- SHRIMP-RG combines the excellent spatial and depth resolution of conventional SIMS with the benefits of extreme mass resolution, while maintaining reproducible, flat-topped peaks and high transmission.

Instrument set-up

- O_2^- primary beam; ~1.5 nA beam current; 15-20 μm spot size
- Yα slits and collector slit closed to achieve M/ΔM >~11000 at 10% peak height, + flat-topped peaks

Mass of interest	Interferences (M/ΔM, calculated from difference between peak centers)
$^{30}Si^+$	$^{29}Si^1H^+$ (2840); $^{28}Si^1H_2^+$ (1590)
$^{31}P^+$	$^{30}Si^1H^+$ (3950)
$^{35}Cl^+$	$^{19}F^{16}O^+$ (1430, guide peak)
$^{43}Ca^+$	$^{27}Al^{16}O^+$ (2430)
$^{45}Sc^+$	$^{90}Zr^{2+}$ (12660); $^{29}Si^{16}O^+$ (2900); $^{28}Si^{16}O^1H^+$ (1890, guide peak)
$^{49}Ti^+$	$^{48}Ti^1H^+$ (6200)
$^{51}V^+$	$^{50}Ti^1H^+$ (5900)
$^{55}Mn^+$	$^{54}Fe^1H^+$ (5860); $^{39}K^{16}O^+$ (2670); $^{23}Na^{16}O_2^+$ (1320)
$^{56}Fe^+$	$^{28}Si_2^+$ (2960), $^{40}Ca^{16}O^+$ (2480)
$^{84}Sr^+$	*$^{42}Ca^{42}Ca^+$ (22050, <0.1%);* $^{44}Ca^{40}Ca^+$ (10800, 4.0%); $^{40}Ca^{28}Si^{16}O^+$ (4000)
✓ $^{86}Sr^+$	*$^{42}Ca^{44}Ca^+$ (17800, <0.2%);* $^{40}Ca^{46}Ti^+$ (14450, 7.8%); $^{40}Ca^{46}Ca^+$ (12270, <0.2%); $^{43}Ca^{43}Ca^+$ (10400, <0.1%); $^{x}Ca^{y}Si^{16}O^+$ (~4000)
$^{88}Sr^+$	*$^{40}Ca^{48}Ti^+$ (17800, 71.6%); $^{44}Ca^{44}Ca^+$ (16480, <0.1%); $^{42}Ca^{46}Ti^+$ (15630, 0.1%); $^{42}Ca^{46}Ca^+$ (13150, <0.1%)*; $^{40}Ca^{48}Ca^+$ (9260, 0.2%); $^{x}Ca^{y}Si^{16}O^+$ (~4100)
$^{89}Y^+$	*$^{40}Ca^{49}Ti^+$ (19350, 5.3%); $^{42}Ca^{47}Ti^+$ (16510, <0.1%); $^{43}Ca^{46}Ti^+$ (16070, 1.0%);* $^{43}Ca^{46}Ca^+$ (13490, <0.2%); $^{x}Ca^{y}Si^{16}O$ (~4200)
$^{93}Nb^+$	*$^{44}Ca^{49}Ti^+$ (30690, 0.1%); $^{43}Ca^{50}Ti^+$ (32980, <0.1%); $^{47}Ti^{46}Ti^+$ (46730, 1.2%); $^{46}Ca^{47}Ti^+$ (100000, <0.1%);* $^{48}Ti^{29}Si^{16}O$ (7170); $^{48}Ca^{29}Si^{16}O$ (5300)
$^{90}Zr^+$	*$^{42}Ca^{48}Ti^+$ (48390, 0.5%); $^{40}Ca^{50}Ti^+$ (33710, 5.2%); $^{44}Ca^{46}Ti^+$ (26470, 0.2%); $^{46}Ca^{44}Ca^+$ (20180, <0.2%); $^{43}Ca^{47}Ti^+$ (15460, <0.1%);* $^{42}Ca^{48}Ca^+$ (13980, <0.2%); $^{46}Ti^{28}Si^{16}O$ (4560); $^{x}Ca^{y}Si^{16}O$ (~4400)
✓ $^{91}Zr^+$	*$^{42}Ca^{49}Ti^+$ (107060, <0.1%); $^{43}Ca^{48}Ti^+$ (84260, 0.1%); $^{44}Ca^{47}Ti^+$ (56880, 0.2%); $^{43}Ca^{48}Ca^+$ (16080, <0.2%);* $^{46}Ti^{29}Si^{16}O$ (4950); $^{46}Ca^{29}Si^{16}O$ (4680)
$^{94}Zr^+$	*$^{44}Ca^{50}Ti^+$ (15290, <0.1%); $^{46}Ti^{48}Ti^+$ (16100, 11.8%); $^{46}Ca^{48}Ti^+$ (19670, <0.1%); $^{46}Ca^{48}Ca^+$ (470000, <0.2%)*
$^{117}Sn^+$	$^{40}Ca^{29}Si^{16}O_3^+$ (5610)
$^{137}Ba^+$	$^{40}Ca^{49}Ti^{16}O_3^+$ (12890)
$^{139}La^+$	$^{44}Ca^{47}Ti^{16}O_3^+$ (9670)
$^{140}Ce^+$	$^{44}Ca^{48}Ti^{16}O_3^+$ (8100)
$^{141}Pr^+$	$^{44}Ca^{49}Ti^{16}O_3^+$ (7200)
$^{181}Ta^{16}O^+$	$^{197}Au^+$ (8520)

Principle mass interferences for trace elements of interest in titanite. Species in *italics* are not resolvable by any mass spectrometer. Tetramers and larger molecular ions, best minimized by energy filtering, are not listed (although those affecting La, Ce and Pr, which can be significant interferences in titanites from some occurrences, are included). Dimers with Al or Fe are also not included. The most problematic Ca-Ca and Ca-Ti dimers interfere with all isotopes of Sr, Y, Nb and Zr, and these are shown in color. Where a % value is given, this is an estimate of dimer abundance relative to $^{40}Ca^{40}Ca^+$ = 94.1% or $^{40}Ca^{48}Ti^+$ = 71.6%. In the cases of Sr and Zr where several isotopes are available, the chosen isotope is denoted by a checkmark, based on a combination of high isotope abundance and minimum dimer interference. For Zr, both $^{90}Zr^+$ and $^{91}Zr^+$ are monitored, but Zr concentration is calculated from $^{91}Zr^+$. Corrections for the unresolvable dimer and Ca-Ti-O interferences on Sr, Y, Zr, Nb, La, Ce and Pr are done by measuring the interferences in synthetic, nominally pure $CaTiO[SiO_4]$ and subtracting observed M^+/Si^+ values from those of the natural samples.

Acquisition set-up and analysis

isotope	amu offset	counting time (s)	Q2 bits	peak centering	notes
$^{7}Li^+$		2	3220	2	
$^{9}Be^+$		2	3160	OFF	
$^{11}B^+$		2	3060	2 first	
$^{19}F^+$		2	2790	2	
$^{23}Na^+$		2	2700	1	
$^{26}Mg^+$		2	2600	1 first	
$^{30}Si^+$		2	2520	3	
$^{31}P^+$		5	2490	3 first	
$^{35}Cl^+$	-0.0245	5	2455	3 first	offset from $^{19}F^{16}O^+$
^{39}K		2	2410	1 first	
$^{43}Ca^+$		2	2375	1	
$^{27}Al^{16}O^+$	+0.0177	2	2375	OFF	offset from $^{43}Ca^+$; Al is measured as an oxide to avoid oversaturating detector
$^{45}Sc^+$	-0.0155	5	2365	1 first	offset from $^{29}Si^{16}O^+$
$^{28}Si^{16}O^1H^+$	+0.00826	1	2365	OFF	offset from $^{29}Si^{16}O^+$
$^{47}Ti^+$		2	2360	1	
$^{51}V^+$		3	2352	1 first	
$^{52}Cr^+$		3	2350	1 first	
$^{55}Mn^+$		2	2340	1 first	
$^{57}Fe^+$		2	2335	1	
$^{59}Co^+$		5	2325	OFF	
$^{60}Ni^+$	-0.0351	5	2320	1	offset from $^{28}Si^{16}O_2^+$
$^{68}Zn^+$		5	2285	OFF	
$^{69}Ga^+$		5	2280	OFF	
$^{74}Ge^+$	-0.02443	2	2265	1	offset from $^{28}Si^{30}Si^{16}O^+$
$^{40}Ca^{40}Ca^+$		1	2230	1 first	monitors Ca dimer production
$^{40}Ca^{42}Ca^+$		1	2225	OFF	monitors Ca dimer production
$^{86}Sr^+$	-0.022	3	2210	1	offset from $^{40}Ca^{30}Si^{16}O^+$
$^{89}Y^+$		3	2195	1	not fully resolvable from several Ca-Ca and Ca-Ti dimers
$^{90}Zr^+$		5	2190	1	not fully resolvable from several Ca-Ca and Ca-Ti dimers
$^{91}Zr^+$		5	2187	1 first	not fully resolvable from several Ca-Ca and Ca-Ti dimers
$^{93}Nb^+$		5	2185	1	not fully resolvable from several Ca-Ca and Ca-Ti dimers
$^{117}Sn^+$		1	2155	OFF	
$^{137}Ba^+$	+0.008	1	2130	OFF	slightly offset from peak center to minimize scattered $^{40}Ca^{49}Ti^{16}O_3^+$ contribution
$^{139}La^+$		5	2125	3	
$^{140}Ce^+$		5	2120	1 first	
$^{141}Pr^+$		5	2115	1 first	
$^{146}Nd^+$		5	2110	1 first	
$^{147}Sm^+$		5	2105	1 first	
$^{153}Eu^+$		5	2100	3 first	
$^{157}Gd^{16}O^+$		5	2095	2	
$^{159}Tb^{16}O^+$		5	2092	OFF	
$^{163}Dy^{16}O^+$		5	2090	3	
$^{165}Ho^{16}O^+$		5	2085	OFF	
$^{166}Er^{16}O^+$		5	2080	3	
$^{169}Tm^{16}O^+$		5	2078	OFF	
$^{172}Yb^{16}O^+$		5	2075	3	
$^{175}Lu^{16}O^+$		5	2073	OFF	
$^{178}Hf^{16}O^+$		5	2070	1 first	
$^{181}Ta^{16}O^+$		5	2065	2 first	
$^{206}Pb^+$		5	2060	2 first	
$^{208}Pb^+$		5	2060	2 first	
$^{232}Th^{16}O^+$		4	2030	3 first	
$^{238}U^{16}O^+$		4	2025	3 first	
96		1	2160	OFF	added to assist stepdown to Li
30		1	2500	OFF	added to assist stepdown to Li
18		1	2800	OFF	added to assist stepdown to Li
11		1	3000	OFF	added to assist stepdown to Li
8		1	3100	OFF	added to assist stepdown to Li

NOTES: Not all isotopes listed are routinely analyzed. *Amu* offset is from guide peak. Q2 bits drift up or down with time (typically in long period [several week] cycles), but the relative differences between masses remain generally the same. OFF means auto-centering is not used and the peak position is adjusted for magnet drift according to the position of the last previously auto-centered peak; numerical value is time (in seconds) taken for auto-centering; "first" means auto-centering is only performed on the first cycle; otherwise, peaks are auto-centered each cycle. Choice of auto-centering, first or always, and auto-centering times have varied over the evolution of the acquisition set-up and may differ slightly between runs.

...characterizing metamorphic reactions

titanite: amphibolite to eclogite facies orthogneiss, ultra-high pressure zone, NE Greenland (courtesy of W. McClelland; sample 03-156)

False-color back-scattered electron (BSE) image of selected titanite grains showing complexity of zoning. Light zones are low average atomic number (low z);dark zones are high average atomic number (high z). Colored ovals are locations of SHRIMP trace element analyses; colors are matched to the eight groups of observed REE patterns.

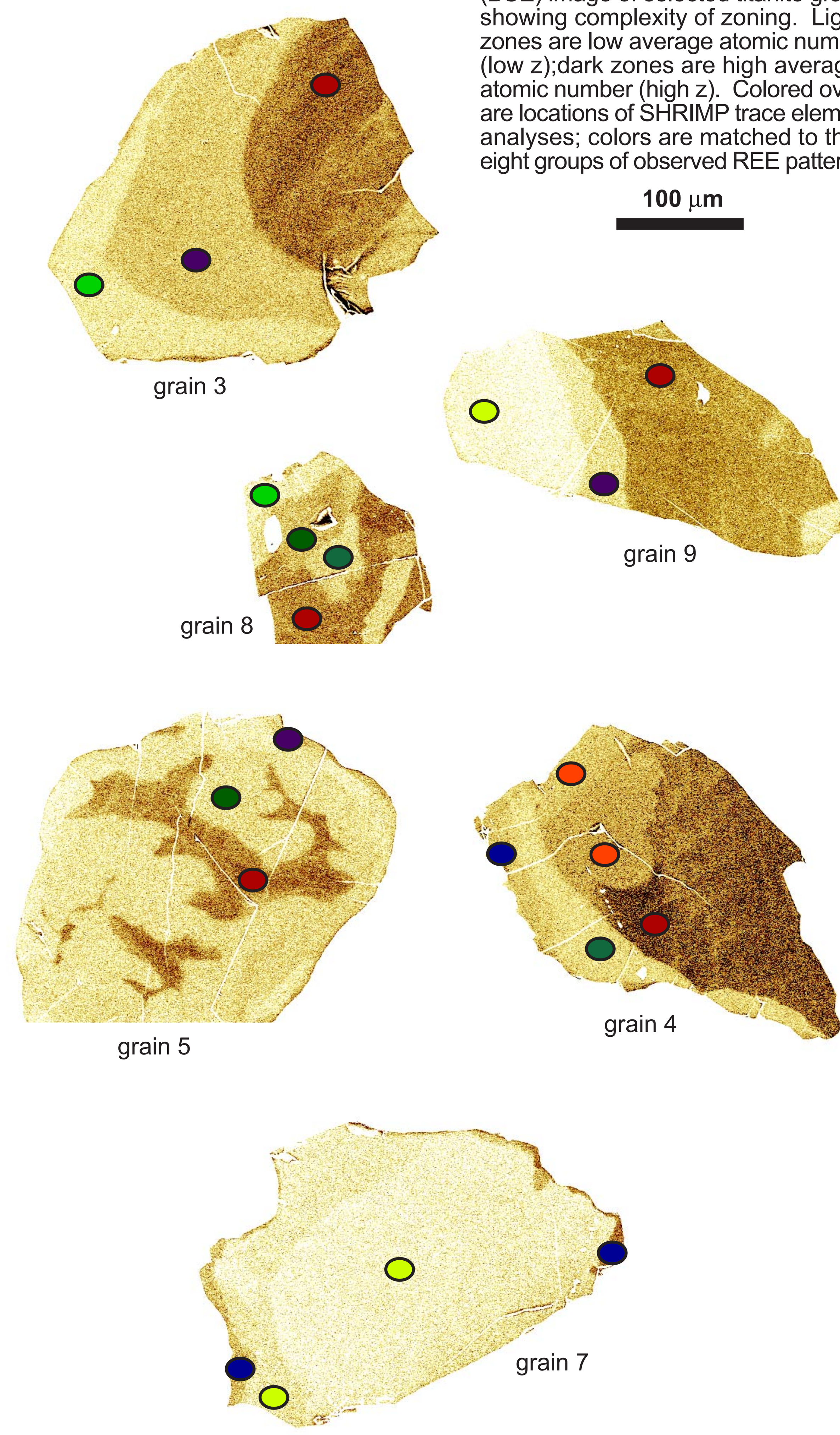

Eight groups of rare earth element (REE) patterns can be distinguished from different BSE zones within sample 03-156. The **red** and **red-orange** groups reflect relict magmatic patterns; the other pattern groups are indicative of later metamorphic reactions. Note the change of scale. The notable and unusual HREE enrichments of the **navy blue** and **plum** groups suggest a garnet breakdown reaction accompanied titanite growth. Plausible mineral reactions accompanying titanite growth, to account for the MREE enrichments of the intermediate green groups, can not be readily discerned from only a grain mount; *in-situ* titanite analysis along with analyses of co-existing phases may yield more definitive evidence and is a direction of further study.

On ternary diagrams of REE distribution, titanite compositions appear to trend first towards MREE enrichment (**green-yellow**, **medium green**, **forest green**, **pine green**) and then to HREE enrichment. However, in some cases (grains 3 & 9), HREE-rich titanite grows directly on relict igneous cores.

...discerning magmatic processes

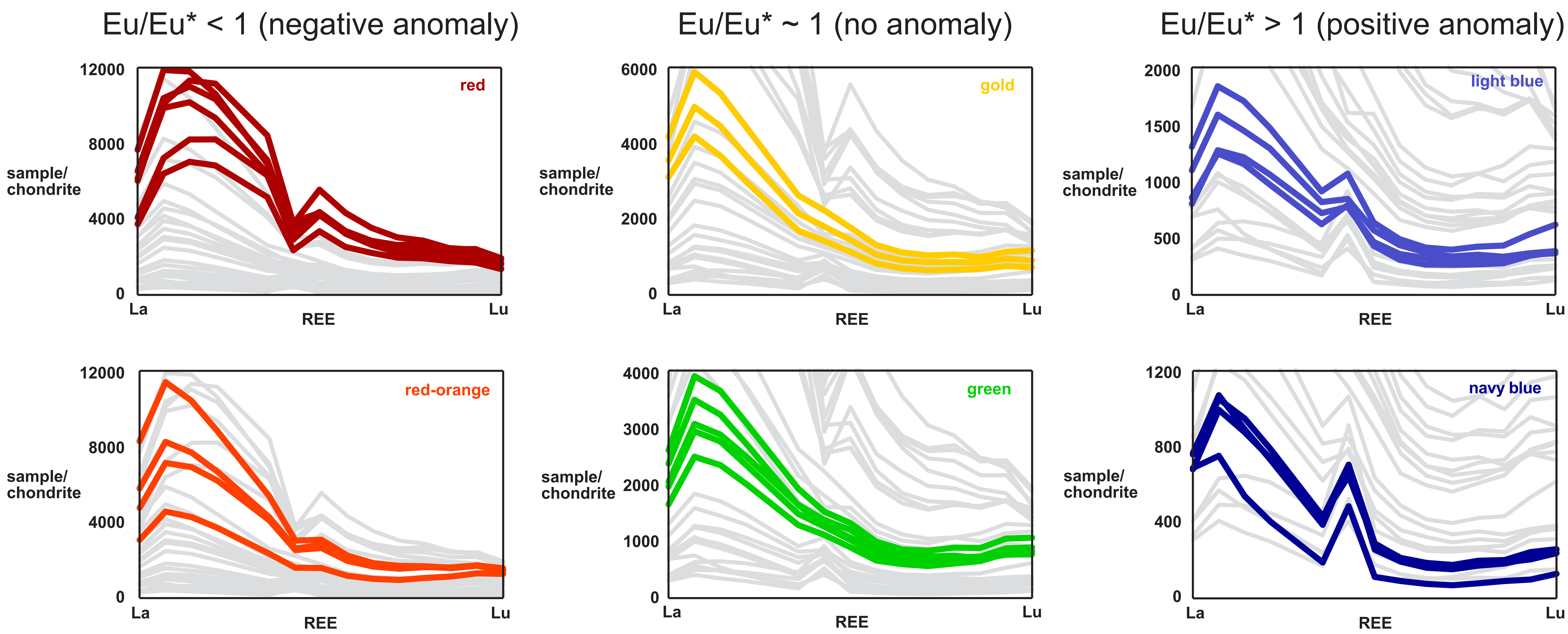

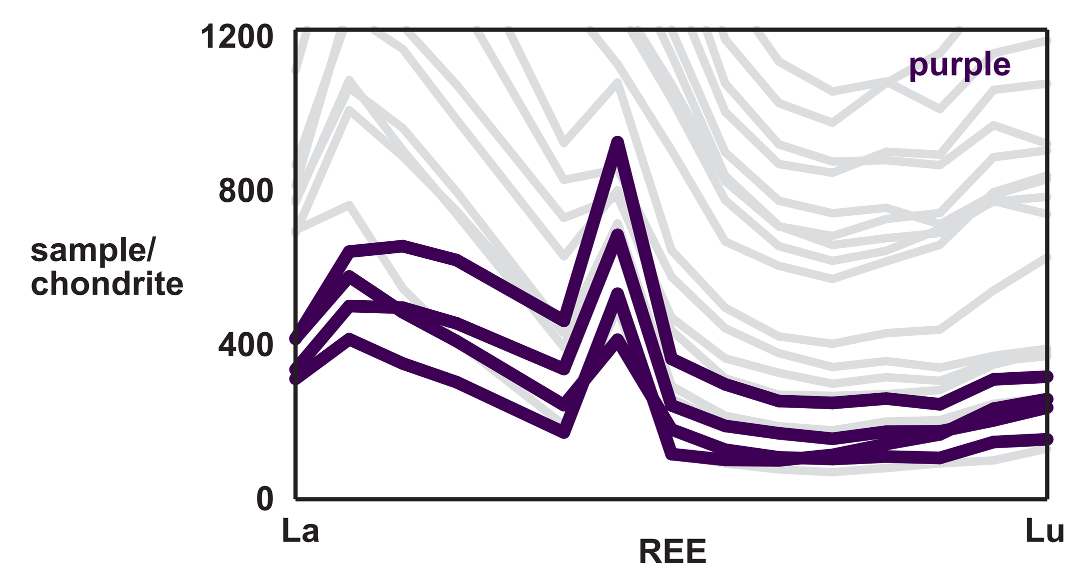

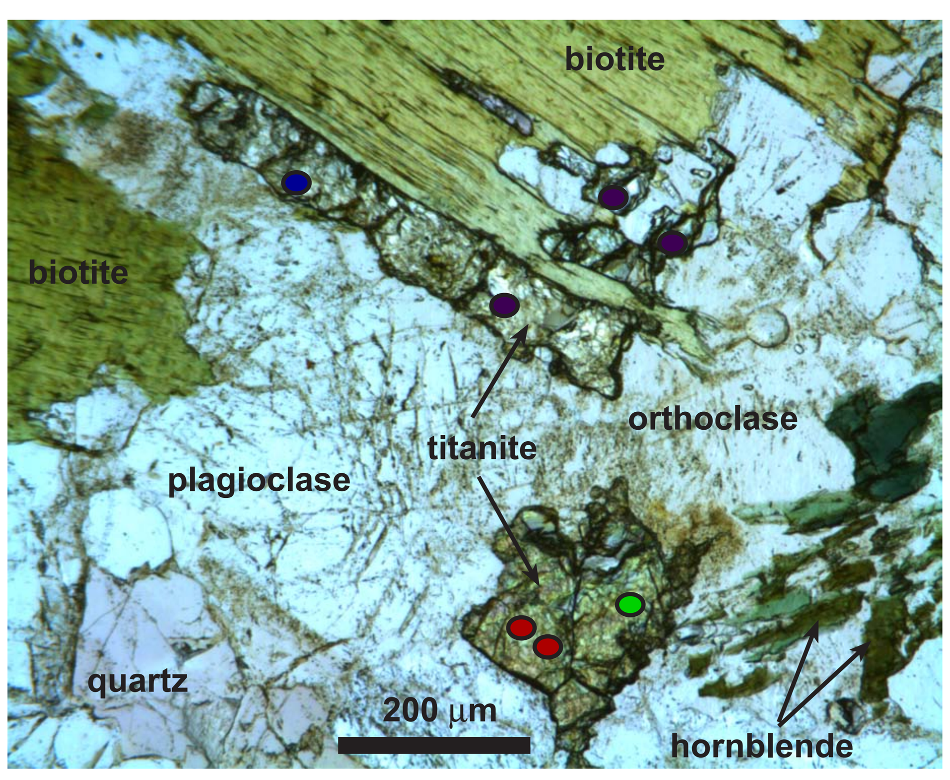

Plane-polarized transmitted light image of JW-198. Colored ovals are locations of SHRIMP trace element analyses; colors are matched to the colored groups of observed REE patterns (above).

titanite: Blue granodiorite, Joshua Tree National Park, CA

(sample JW-198)

Seven groups of REE patterns can be differentiated from among the different grains and BSE-visible compositional zones in titanite from JW-198. Note the change of scale. The patterns are characteristically sub-parallel and show Eu/Eu* transitioning from negative to positive with decreasing temperature. A marked transition in titanite Th/U occurs ~750 °C and indicates a large-scale physio-chemical change in the magma or a new titanite-forming event.

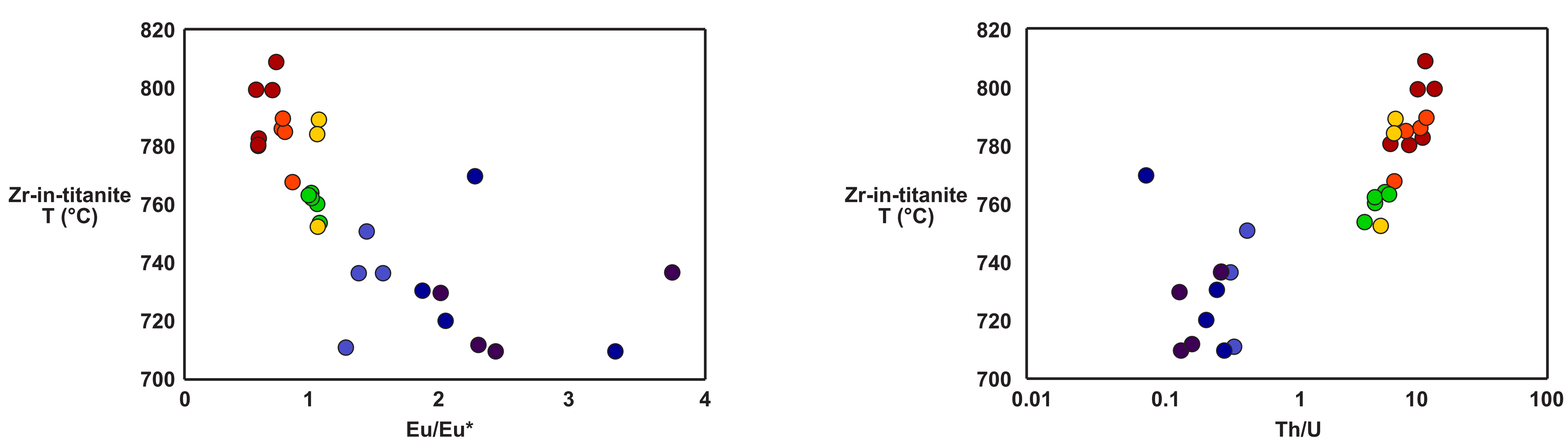

Plots of Zr-in-titanite temperatures vs. Eu/Eu* and Th/U for titanite from JW-198. Calibration for Zr-in-titanite thermometer comes from Hayden *et al.* (abstract: Goldschmidt conference, 2006). Pressure estimate is 0.5 GPa. Symbol coloration corresponds to the REE pattern colors (above).

...describing the nature of hydrothermal fluids

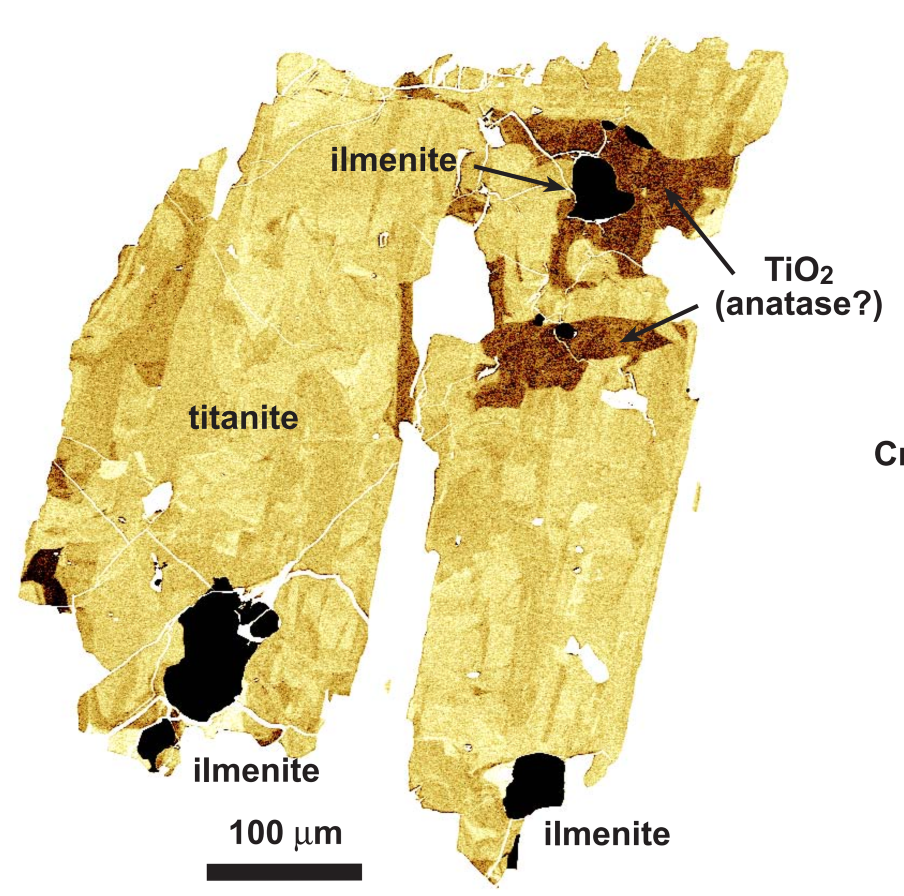

False-color back-scattered electron (BSE) image of relict(?) magmatic ilmenite replaced by hydrothermal titanite+anatase(?), from actinolite-albite-titanite veins cutting Na-Ca metasomatized diorite, Duff Creek, Cortez Mountain metasomatic iron-oxide-Cu-Au (IOCG) district, NV.

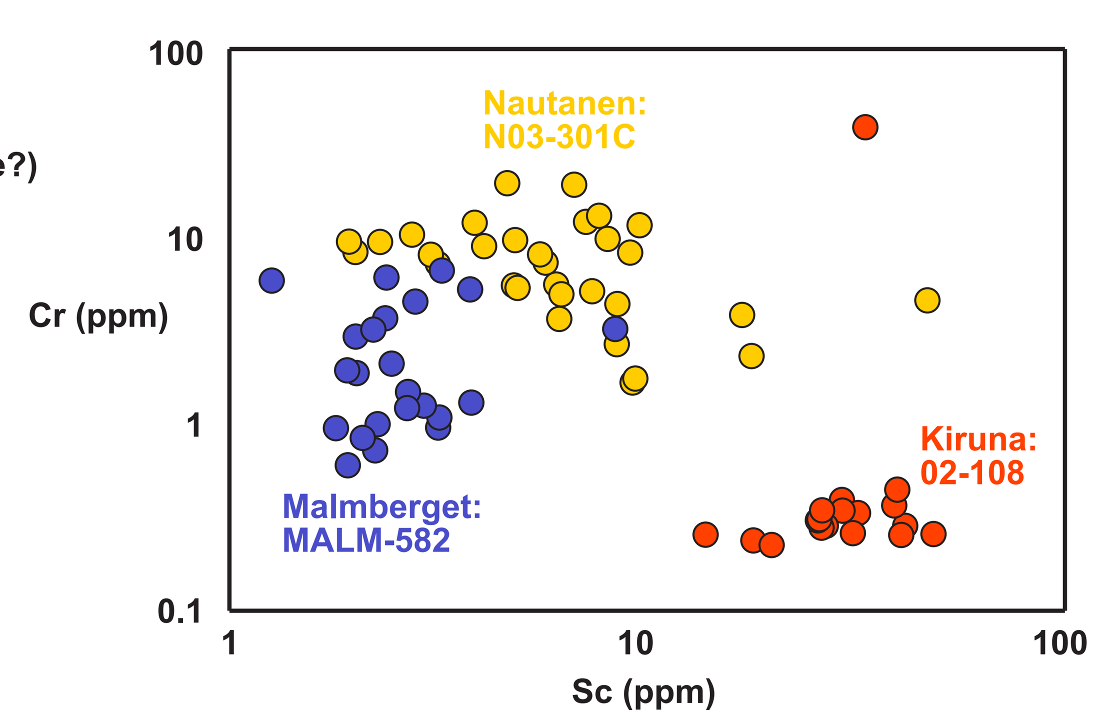

Cr and Sc concentrations of titanite from three Swedish metasomatic iron-oxide-Cu-Au (IOCG) deposits. (samples courtesy of D. Johnson. 02-108 comes from magnetite-actinolite-titanite breccia ore; N03-301C comes from actinolite-bornite-albite-titanite veins cutting meta-andesite; MALM-582 comes from pervasive albite-actinolite alteration of a felsic(?) volcanic rock).

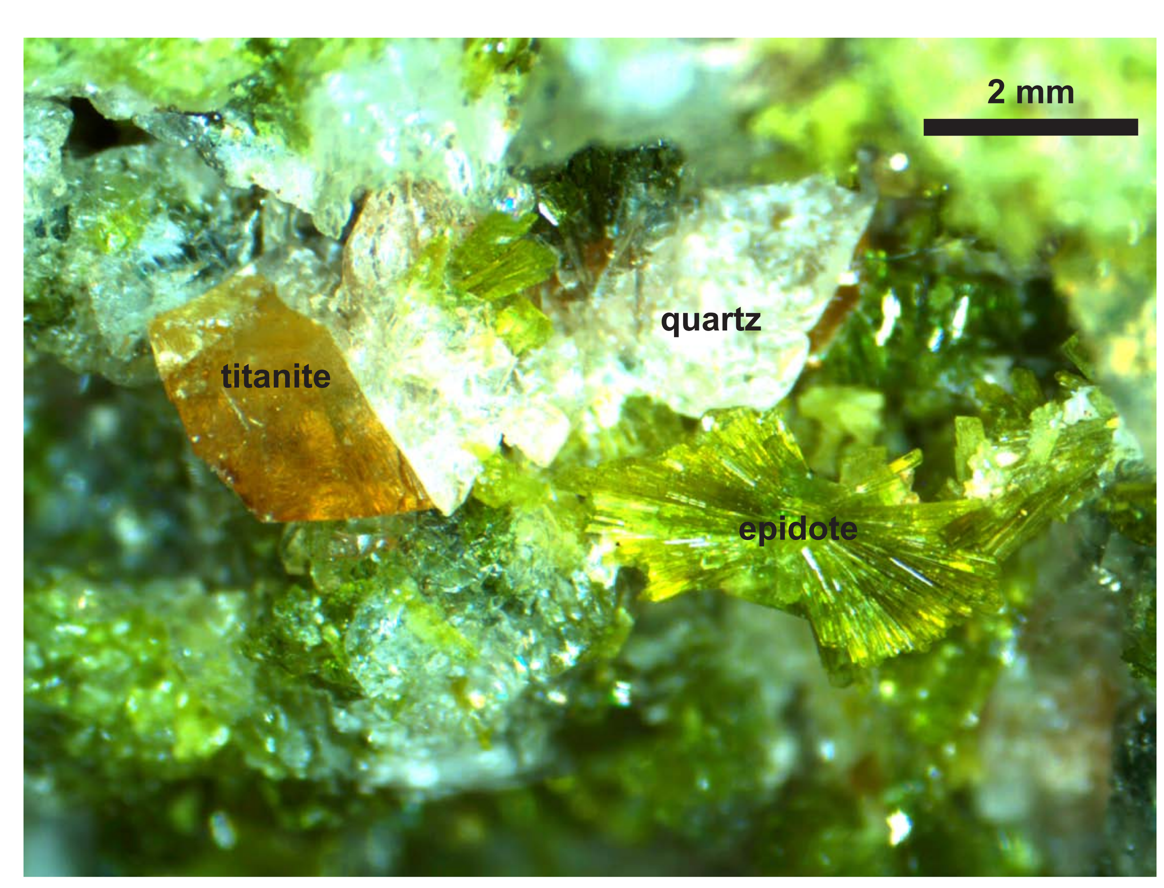

Titanite-epidote-quartz-(actinolite-calcite) from calcic alteration assemblage, Imilchil metasomatic iron-oxide-Cu-Au (IOCG) system, High Atlas Mountains, Morocco.

Hydrothermal titanite can show significant compositional diversity, reflecting variations in fluid chemistry and host rock composition. These examples from metasomatic iron-oxide-Cu-Au (IOCG) occurrences illustrate some of the variety of mineralogical, textural and compositional features observed.